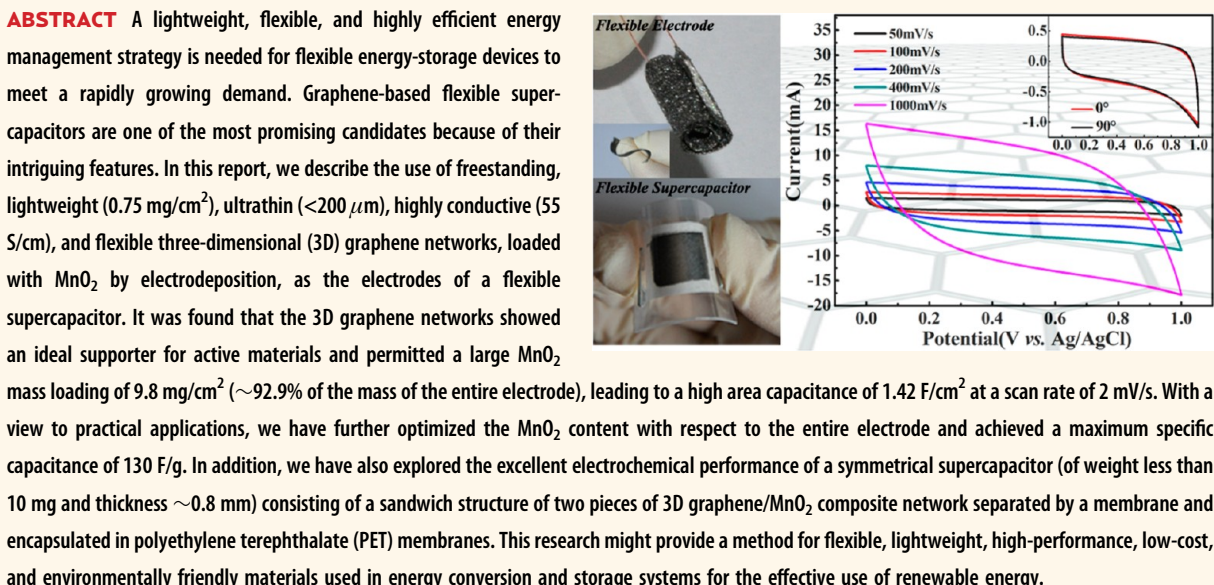


Freestanding Three-Dimensional Graphene/MnO₂ Composite Networks As Ultralight and Flexible Supercapacitor Electrodes

Yongmin He,^{†,*} Wanjun Chen,[†] Xiaodong Li, Zhenxing Zhang, Jiecai Fu, Changhui Zhao, and Erqing Xie^{*}

School of Physical Science and Technology, Lanzhou University, Lanzhou 730000, People's Republic of China. [†]These authors contributed equally to this work.



KEYWORDS: graphene · 3D conductive network · flexible · ultralight · MnO₂ · supercapacitor

During the past years, a significant amount of effort has been devoted to flexible energy storage materials because of their potential applications in portable electronic devices, such as roll-up displays, electronic paper, wearable devices, mobile phones, and computers.^{1–4} The emerging flexible supercapacitors, with higher energy density than conventional physical capacitors, higher charging/discharging rate capability, and longer life-cycles than primary/secondary batteries, have become one of the most intense research focuses in the electrical energy storage field.^{5–7} Generally, to make flexible energy conversion/storage devices, a freestanding and binder-free electrode with favorable mechanical strength and large capacitance is required to provide a vital component for flexible supercapacitors. In this point of view, carbon materials have shown great

potential as the electrodes of flexible supercapacitors owing to their superior mechanical properties and excellent electrochemical double-layer capacitor performance.⁸ Since electrodes constructed from transition metal oxides and conducting polymers are prone to fracture under slight tensile strain, papers, films, and even cloth fabricated using carbon nanotubes (CNTs)/nanofibers (CNFs) have been studied for their suitability as freestanding flexible electrodes.^{9–11} In most cases, carbon-based materials are used as the backbone materials, in combination with electroactive materials, including conducting polymers¹² and transition metal oxides^{13–15} (such as RuO₂, Co₃O₄, and MnO₂) for pseudocapacitor electrodes to achieve ultrahigh values of electrode capacitance.

Among those carbon materials, graphene has attractive characteristics, such as large

* Address correspondence to
heyongming11@163.com (Y.H.),
xieeq@lzu.edu.cn (E.X.).

Received for review August 4, 2012
and accepted December 18, 2012.

Published online December 18, 2012
10.1021/nn304833s

© 2012 American Chemical Society

surface, high flexibility, excellent electrical conductivity, good chemical and thermal stability, wide potential windows, and abundant surface functional groups.^{16,17} Moreover, self-supporting graphene papers (or films) show great potential as flexible electrodes with excellent mechanical stiffness and strength.^{18–20} However, in most cases, graphene nanosheets (GNS) were assembled into macroscopic paper-like structures in a way that reduced the large accessible surface area of the two-dimensional (2D) GNS. This usually results from irreversible agglomeration and restacking of the individual GNS. These drawbacks hinder potential applications of graphene materials in electrochemical electrodes, composite materials, and so on. Recently, some improvements were made by incorporating spacers such as CNTs,^{21,22} CNFs,²³ transition metal oxides,²⁴ and conducting polymers^{25–27} into graphene papers (or films) to expand the layers' distance between the sheets of graphene papers (or films). However, inherent drawbacks of graphene papers (or films) still exist in two aspects: (1) irreversible agglomeration and restacking of GNS caused by the strong π – π interactions and van der Waals force between the planar basal planes of the GNS and (2) low specific surface area of the paper (or film) due to its 2D structure. More recently, freestanding 3D graphene nanostructures constructed by GNS through self-assembled^{28,29} or templated assembly³⁰ methods have been reported. These graphene nanostructures showed a well-defined and cross-linked 3D porous structure and a remarkably high specific surface area. In most cases, the weak contact between GNS has led to poor conductivity and mechanical properties of the electrode, further reducing their performance as flexible supercapacitors. To alleviate these problems, a promising freestanding 3D graphene structure was produced by chemical vapor deposition (CVD) growth with Ni foam as a 3D template.^{31,32} The resultant 3D graphene structure showed a very high conductivity due to the absence of defects and intersheet junction contact resistance, as well as a high specific surface area for its porous structure. However, this 3D structure (without supporter) still exhibited a poor flexibility and collapsed and cracked easily during bending operation due to the hollow internal structure and sparse skeletons, which greatly limited its application as electrodes of flexible supercapacitors. Therefore, it is still an urgent and important issue to find efficient ways to resolve the aforementioned problems, providing an ideal graphene-based electrode for flexible supercapacitors with outstanding flexibility, high conductivity, and large specific surface area.

Of the electro-active materials mentioned above, MnO_2 has appeared as one of the most promising candidates due to its low cost, high electrochemical activity, and environmentally friendly nature.^{33,34} However, the intrinsically poor electrical conductivity

(10^{-5} – 10^{-6} S/cm) of MnO_2 is a hindrance to obtain high electrochemical performance. To improve the electrical conductivity of MnO_2 -based electrodes, hybrid graphene/ MnO_2 nanostructures are being developed for large-scale energy storage systems.^{24,35,36} In large capacitor applications such as power sources for hybrid electric vehicles or fuel cell electric vehicles, a large mass loading of MnO_2 is needed.^{37,38} Unfortunately, the high mass loading always leads to a decrease of specific capacitance due to close-packed structures resulting in a limited electrochemically active surface area, so only ultrathin layers of MnO_2 (with thickness often $<1\ \mu\text{m}$) can deliver very high specific capacitances.

In this work, we report a type of MnO_2 -coated freestanding, flexible, lightweight, and highly conductive 3D graphene network, of which the remarkably high specific surface area ($392\ \text{m}^2/\text{g}$) allows an extremely large mass loading of 92.9% MnO_2 (measured content for the entire electrode). These hybrid flexible electrodes exhibit a high areal capacitance of $1.42\ \text{F}/\text{cm}^2$ and a high specific capacitance of $130\ \text{F}/\text{g}$ (calculated for the entire electrode). Moreover, this type of simply fabricated supercapacitors possesses remarkable electrochemical performance and excellent mechanical properties.

RESULTS AND DISCUSSION

Figure 1a shows the fabrication process for the 3D graphene networks. First, a piece of commercially available Ni foam (37.5 – $40\ \text{mg}/\text{cm}^2$) was pressed into a $\sim 0.2\ \text{mm}$ thick sheet. Figure 1a(1, 2) shows digital photos of the Ni foams before and after pressing, respectively. The pressed Ni foam was then cleaned successively in 1 M hydrochloric acid, acetone, and deionized water. The Ni foam was subsequently coated with graphene by atmospheric pressure chemical vapor deposition (AP-CVD), upon which the color of the Ni foam changed from shiny white to dark gray (Figure 1a(3)). After removal of the Ni foam, a 3D graphene with a foam-like network was obtained, with a weight of 0.70 – $0.75\ \text{mg}/\text{cm}^2$ and thickness less than $200\ \mu\text{m}$ (Figure 1a(4)). The freestanding 3D graphene networks obtained in this way from pressed Ni foam show greater flexibility and superior mechanical strength in comparison to those from nonpressed foam, as reported elsewhere,^{31,32,39} as shown in Figure 1b and Figure S1. In addition, these 3D graphene networks exhibit a higher electrical conductivity of $55\ \text{S}/\text{cm}$ than other 3D conducting structures.^{28,30,33,38} It is necessary to point out that the 3D graphene network skeleton possesses a hollow internal structure that is the same as that present in the Ni foam (Figure S2a, b). This means that the 3D structure collapses and cracks easily during bending operation due to the hollow internal structure and sparse skeletons (Figure S2c, d). To solve those problems, we press the Ni foam to make a compact 3D structure, giving four advantages: (1) maintenance of the

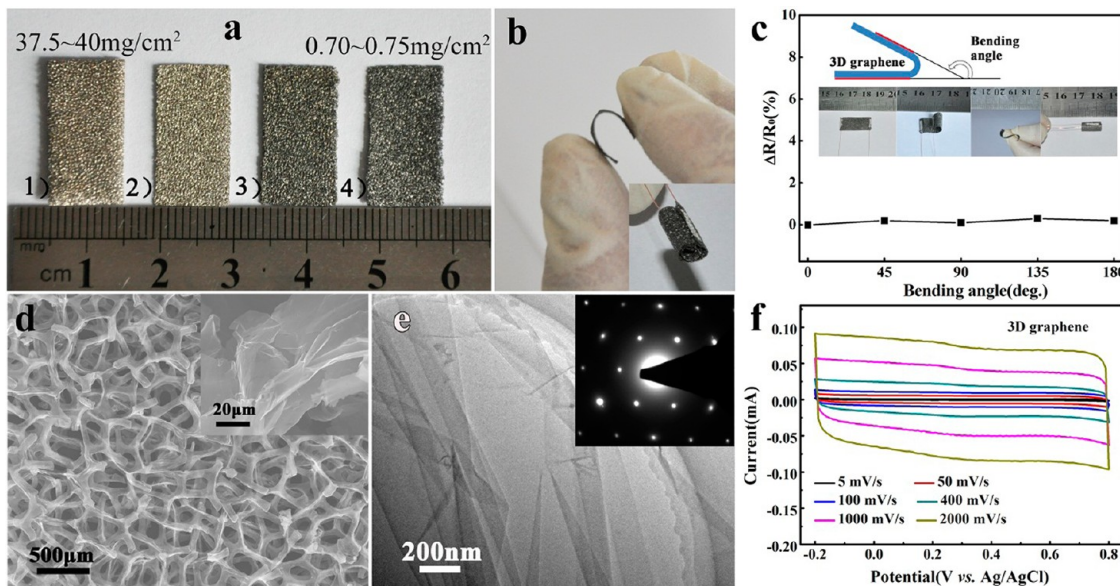


Figure 1. (a) Digital photographs of Ni foams with (1) and without (2) pressed and graphene-coated Ni foams before (3) and after (4) removal of the Ni networks. (b) Digital photograph of a freestanding and flexible 3D graphene network prepared from pressed Ni foam. Inset shows the curled 3D graphene networks. (c) Electrical-resistance variation of 3D graphene networks *vs* the different bending angles. Inset shows the digital photographs of different bending shapes. (d) SEM image of 3D graphene networks after removal of Ni foam. Inset shows high-magnification SEM image. (e) TEM image of a graphene sheet. Inset shows a SAED pattern of the corresponding GNS. (f) CVs of the 3D graphene network electrode in 0.5 M aqueous Na_2SO_4 electrolyte at different scan rates.

3D structure for the graphene networks, with no cracks or collapsing owing to the strength and ductility of Ni metal (Figure S3); (2) reduction of the size of the pores and the thickness of the Ni foam, which results in a lower volume for the 3D graphene network, as shown in Figure S2b and Figure S3b; (3) improvement of the flexibility of the 3D graphene network and its ability to suffer a large deformation; (4) allowing a uniform electrodeposition of the MnO_2 nanostructure material on the 3D graphene network by shortening the diffusion distance of the solution, due to its hydrophobic property (Figure S4). To further demonstrate the good mechanical properties of our 3D graphene networks prepared from pressed Ni foam, we measured its electrical-resistance variation *versus* the different bending angles with a range of angles from 0° to 180° (Figure 1c). Under the different degrees of mechanical deformation used in this test, there are little change (less than 1%) of the electrical resistance at the different bending angles. Moreover, the 3D graphene networks in our work possess foldable, flexible, and curved properties, as shown in Figure 1c (inset). In addition, the electrical resistance of 3D graphene networks as a function of the number of bending cycles was also measured, and the electrical resistance was slightly increased after 500 bending cycles (Figure S5). Herein, this simple method provides a useful approach to prepare 3D graphene networks with the highlights of good flexibility and conductivity.

The morphology and structure of the 3D graphene networks were examined by scanning electron microscopy

(SEM) and transmission electron microscopy (TEM), as shown in Figure 1d and e, respectively. As shown in Figure 1d, after removal of the Ni template, the graphene replicates the 3D network and porous structure of the pressed Ni foam, without collapsing and cracking. Figure 1e shows the TEM image of a graphene sheet, and the number of layers is 4–7 in our experiment, as shown in Figure S6. The selected area electron diffraction (SAED) pattern (inset of Figure 1e) gives reflection spots arranged in a typical hexagonal pattern, confirming the formation of high-quality graphene after AP-CVD. To explore the advantages of 3D graphene as an active electrochemical capacitor electrode, Figure 1f shows the cyclic voltammograms (CVs) for bare 3D graphene networks over a range of scan rates from 5 to 2000 mV/s. The CVs retain a nearly symmetrical rectangular shape within the range of scan rates employed, which is characteristic of electrochemical double-layer capacitive behavior. Therefore, we can deduce that the 3D graphene networks formed from the pressed Ni foam can be used as freestanding flexible electrodes, which would provide an ideal support for active materials.

We have deposited nanostructured MnO_2 materials on 3D graphene networks through an electrochemical deposition process. The mass loading of MnO_2 can be well controlled by adjusting the deposition current and deposition time. As shown in Figure 2a, the mass loading increased linearly with deposition time at an applied square-wave pulse current of $500 \mu\text{A}/\text{cm}^2$, while the MnO_2 content (the weight percentage of

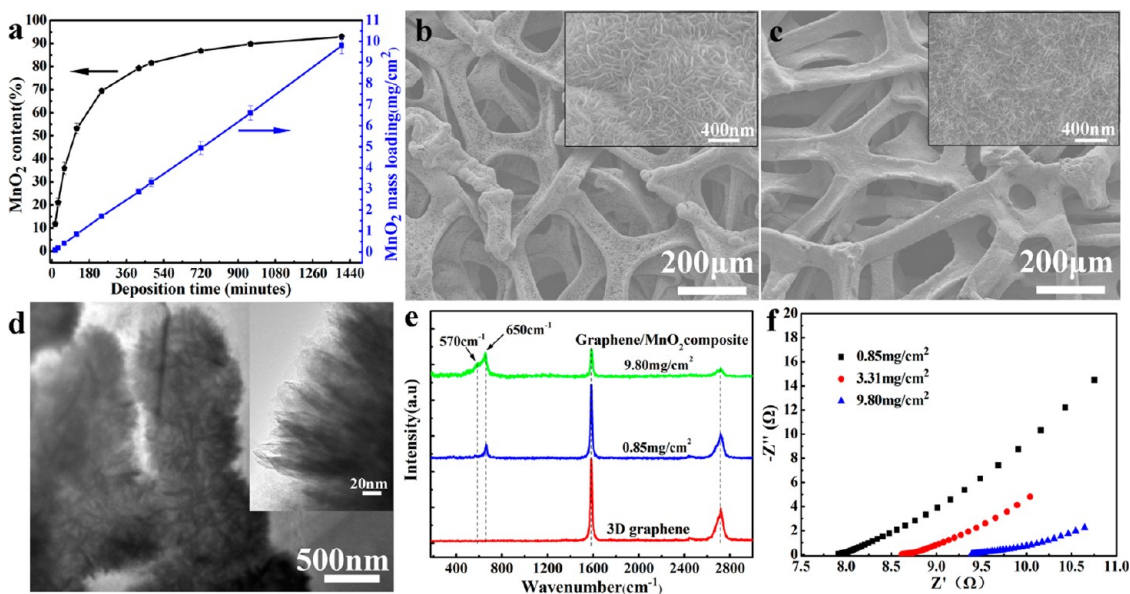


Figure 2. (a) MnO₂ content and mass loading vs electrodeposition time from 15 to 1440 min. (b and c) SEM images of two typical samples with mass loadings of 0.85 mg/cm² (b) and 9.8 mg/cm² (c) showing uniform coating of MnO₂ inside and outside the 3D graphene networks. The insets are the corresponding high-magnification SEM images of two typical samples. (d) TEM image of the nanoporous structure of MnO₂ with a deposition time of 120 min. The inset is the high-magnification TEM image. (e) Raman spectra of the 3D graphene networks and the graphene/MnO₂ composite with MnO₂ mass loadings of 0.85 and 9.8 mg/cm². (f) Nyquist plot of the graphene/MnO₂ composite electrode with a range of MnO₂ mass loadings.

MnO₂ in the graphene/MnO₂ composite) follows a logarithmically rising behavior. The average deposition rate is calculated to be $\sim 6.7 \mu\text{g}/\text{min}$ by linearly fitting the data. Due to the remarkably high specific surface area (392 m²/g) of the 3D graphene networks, a large MnO₂ mass loading of 9.8 mg/cm² can be achieved by increasing the deposition time to 1440 min, to give a corresponding content of 92.9%, which is much higher than the value reported previously.^{37,38,40}

Figure 2b and c show the low- and high-resolution SEM images of two typical samples, with mass loadings of 0.85 and 9.8 mg/cm². It is observed that the MnO₂ nanomaterials were uniformly coated over almost the entire skeletons of the 3D graphene networks. The MnO₂ shows a hierarchical nanosphere structure, consisting of MnO₂ nanosheets for a deposition time of less than 120 min, a result further confirmed by the TEM image shown in Figure 2d. Moreover, the electrodeposition can provide a nanoporous structure of MnO₂ on the 3D graphene networks with large range deposition times from 15 to 1440 min, as shown in Figure S7. This type of nanoporous structure produces large accessible surface areas that enable effective electrolyte ion transport during supercapacitor operations, agreeing with other previous studies.³³ The crystallinity of the electrodeposited MnO₂, with mass loadings of 0.85 and 9.8 mg/cm², was determined by Raman spectroscopy and XRD patterns, as shown in Figure 2e and Figure S8, respectively. Except for the characteristic G and 2D peaks at ~ 1575 and 2740 cm^{-1} from graphene, two other peaks were observed at 570 and 650 cm^{-1} , which are characteristic peaks of the

Mn–O lattice.⁴¹ The intensity of the MnO₂ peaks increases, in contrast to those of graphene, as the MnO₂ mass loading increases. Preliminary results show that only the outer surface of the graphene networks prepared from nonpressed Ni foam became coated with MnO₂ (Figure S9). This results from the lack of hydrophilic groups for 3D graphene networks. Due to the surface tension, the solution would be prevented from diffusing to the inner part of 3D graphene networks. However, the nonuniform electrodeposition (only the outer surface) of MnO₂ in the networks can be relieved by using the method of reducing the thickness of the networks to shorten the diffusion distance of the solution. As a result, the MnO₂ was coated uniformly over the entire surface of the 3D graphene networks prepared from pressed Ni foam, as shown in Figure 2b and c and Figure S7.

Figure 2f shows a Nyquist plot of the graphene/MnO₂ composite electrode in a 0.5 M Na₂SO₄ electrolyte solution. These measurements were carried out at room temperature in the frequency range 0.1 Hz to 100 kHz at open-circuit voltage, with an ac amplitude of 5 mV. On the Nyquist plot, the intercept at the real part (Z') is a combination of the ionic resistance of the electrolyte, the intrinsic resistance of the substrate, the intrinsic resistance of the active material, and the contact resistance at the active material/current collector interface. The ionic resistance of the electrolyte was $\sim 5.4 \Omega$, measured using the three-electrode system with Pt as the working electrode and without MnO₂ deposition. The resistance of the graphene/MnO₂ composite electrode can be calculated by subtracting

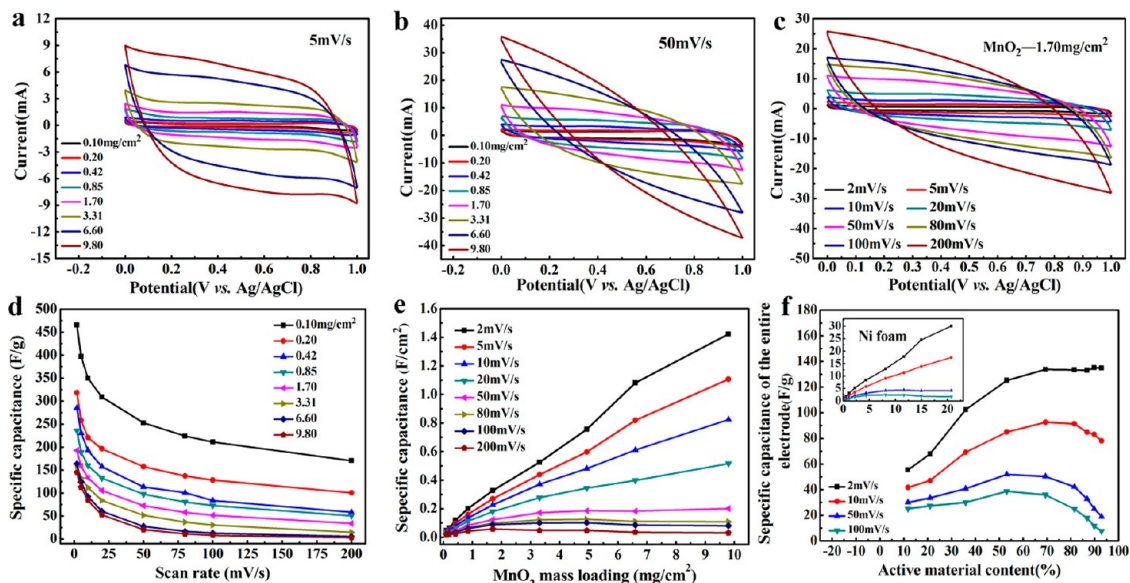


Figure 3. (a, b) CVs of graphene/MnO₂ composite electrode with different areal mass densities of MnO₂ at scan rates of (a) 5 mV/s and (b) 50 mV/s. (c) CVs of a graphene/MnO₂ composite electrode with a fixed areal mass density of 1.70 mg/cm² at different scan rates. (d) Specific capacitance vs scan rate for samples with different areal mass densities of MnO₂. (e) Areal capacitance vs areal mass densities of MnO₂ at different scan rates. (f) Specific capacitance of the entire electrode vs the content of active material (MnO₂) for the entire graphene/MnO₂ composite electrode at different scan rates. Inset shows specific capacitance of the entire electrode vs the content of active material (MnO₂) for the entire Ni foam/MnO₂ composite electrode at different scan rates.

the ionic resistance of the electrolyte from the value of Z' and is 2.41, 3.22, and 4 Ω for 0.85, 3.31, and 9.80 mg/cm² MnO₂ mass loading, respectively. These values suggest good contact between the MnO₂ and 3D graphene networks. In this work, the increase in the resistance is mainly attributed to the low conductivity of MnO₂.

In order to evaluate the contribution of MnO₂ to the capacitance of the graphene/MnO₂ composite electrodes, we carried out a detailed study of the impact of the mass loading (0.1–9.8 mg/cm²) or the mass content (11.7–92.9%) within a large range of scan rates on the capacitance. We first performed CV scans of the graphene/MnO₂ composite electrode with the MnO₂ deposition time ranging from 15 to 1440 min, resulting in the corresponding MnO₂ content varying from 0.1 to 9.8 mg/cm², at scan rates of 5 and 50 mV/s, as shown in Figure 3a and b, respectively. The current response increases with an increase in MnO₂ mass at both scan rates, indicating an increase of the total capacitance. To further investigate the influence of the scan rates on the capacitance, we measured the CVs of the graphene/MnO₂ composite with 1.70 mg/cm² MnO₂ at various scan rates, from 2 to 200 mV/s, as shown in Figure 3c. As the scan rate increases, the peak current increases, while the shape of the curve deviates from the rectangular shape of an ideal capacitor because of the overpotential. The specific capacitances, as a function of the different masses of MnO₂, are plotted in Figure 3d. For this plot, the specific capacitance of MnO₂ was calculated by subtracting the charge of the bare 3D graphene networks, of which the value is small

due to its limited electro-active sites and hydrophobic property. The highest specific capacitance is 465 F/g for the sample with a mass loading of 0.1 mg/cm² at a scan rate of 2 mV/s, which is higher than literature values.³⁸ The decrease of the specific capacitances with increasing MnO₂ mass loading is due to (1) the additional MnO₂, especially the portion far away from the surface, not actively participating in pseudocapacitive reactions due to a low proton diffusion constant ($\sim 10^{-13}$ cm²/(V s)) and (2) lowering of the electrical conductivity of the graphene/MnO₂ composite due to the increase of MnO₂ with its low conductivity of 10^{-5} – 10^{-6} S/cm.

The mass loading per area is shown in Figure 3e and gives another important characteristic of the supercapacitors. At low scan rates (<20 mV/s), the capacitance increases with the increase of MnO₂ mass and no saturation appears, indicating that almost all the MnO₂ contributes to the energy storage. This can be attributed to both the 3D porous structures of graphene and the porous structure of the MnO₂ nanomaterials, allowing a smaller resistance and the possibility of micrometer-scale diffusion pathways. At scan rates of 50–200 mV/s, the areal capacitance increases with the mass loading until a critical value is reached at approximately 3.31 mg/cm², which is larger than reported elsewhere.³⁸ The existence of this critical value may be because the thickness of MnO₂ corresponding to the critical mass is close to the Na⁺ diffusion length at these scan rates for this particular graphene/MnO₂ composite electrode. At the device level, the high performance of the supercapacitors depends critically

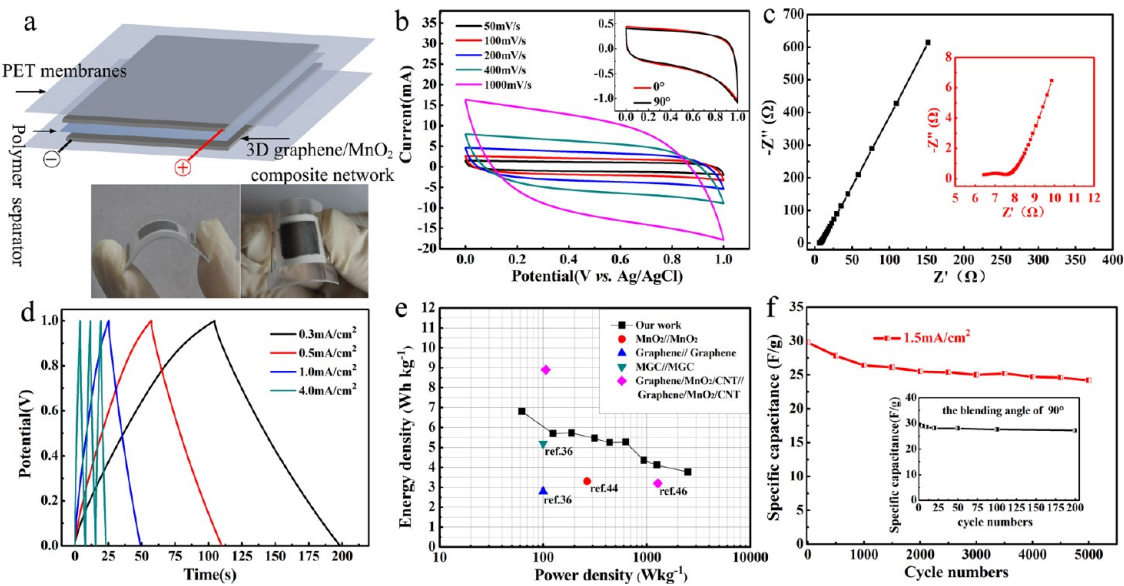


Figure 4. (a) Schematic of the structure of our flexible supercapacitors consisting of two symmetrical graphene/MnO₂ composite electrodes, a polymer separator, and two PET membranes. The two digital photographs show the flexible supercapacitors when bended. (b) CVs of the flexible supercapacitors at scan rates of 50, 100, 200, 400, and 1000 mV/s. Inset shows the CVs of the flexible supercapacitors with bending angles of 0° and 90° at a fixed scan rate of 10 mV/s. (c) Nyquist plot of the flexible supercapacitor. (d) Galvanostatic charging/discharging curves of the flexible supercapacitor device at different current densities. (e) Ragone plots of the flexible supercapacitor, compared with the values of similar symmetrical systems from refs 36, 44, and 46. (f) Cycling performance of the flexible supercapacitors for charging and discharging at a current density of 1.5 mA/cm². Inset shows cycling performance of the flexible supercapacitors for bending cycles with a bending angle of 90°.

on the total mass, including all the components in the device (electrolyte, current collectors, electrodes, separator, packaging, etc.). Thus, the mass of the active material (MnO₂ in our study) with respect to the combined mass of electrodes and current collectors must be optimized when considering the maximum contribution to the capacitance of the entire electrode. As shown in Figure 3f, the specific capacitance of the entire electrode increases with the increase of the content of active material and reaches a maximum value for an active material content of 55–75%, for scan rates of 2, 10, 50, and 100 mV/s. At the lowest scan rate of 2 mV/s, the specific capacitance of the entire electrode remains as high as 130 F/g even when the mass of active material is up to 92.9%, indicating that the active materials in our hybrid structure have an excellent capability to contribute to the capacitance of the entire electrode owing to the lightweight nature and high electrochemical performance of the graphene/MnO₂ composite electrode. In order to compare the contribution of the active materials to the capacitance, MnO₂ was also electrodeposited onto Ni foams using deposition times ranging from 15 to 1440 min under the same conditions used for the 3D graphene networks. A remarkably low contribution for the Ni foam electrode was demonstrated, in comparison with that of 3D graphene networks, as shown in the inset of Figure 3f. These results demonstrate that the strategy for designing a device must be to optimize the active material (MnO₂) mass content over the

entire electrode. This will improve the performance of the supercapacitors.

To further explore the advantages of this novel design for real applications, a supercapacitor was assembled from two pieces of 3D graphene/MnO₂ composite networks, each with a mass loading of 0.4 mg/cm². The assembled supercapacitor was lightweight (less than 10 mg), thin (~0.8 mm), and highly flexible, as shown in Figure 4a. The rectangular shapes and symmetry of the CV scans indicate its ideal pseudo-capacitive nature, even at the high scan rate of 1000 mV/s, as shown in Figure 4b. In order to demonstrate the flexibility of our device, we measured CV curves at the scan rate of 10 mV/s with a bending angle of 90°. As shown in the inset of Figure 4b, there is no significant difference between the CV curves with and without bending, suggesting the high flexible property for the 3D graphene/MnO₂ composite network-based symmetrical supercapacitor. The series resistance of the device is ~6.4 Ω, as determined from the Nyquist plot in Figure 4c, indicating a low internal resistance for the whole device. A galvanostatic charging/discharging test was also performed with different current densities over the voltage window of 0–1 V, as shown in Figure 4d. The linear voltage versus time profiles, the symmetrical charge/discharge characteristics, and a quick *I*–*V* response represent good capacitive characteristics for our supercapacitor.

The flexible supercapacitor exhibits an energy density of 6.8 Wh/kg at a power density of 62 W/kg for a 1 V

window voltage, as shown in Figure 4e. It also preserves 55% of its energy density as the power density increases to 2500 W/kg. These values are superior to the similar previously reported symmetrical systems graphene//graphene (2.8 Wh/kg),³⁶ MnO₂/graphene composite (MGC)/MGC (5.2 Wh/kg),³⁶ and MnO₂//MnO₂ supercapacitors with a cell voltage of 0.6–1.0 V (1.9–3.3 Wh/kg).^{42–44} A rough comparison indicates that these values are also competitive with those of other MnO₂-based symmetric flexible electrochemical capacitors, such as carbon nanoparticles/MnO₂ (4.8 Wh/kg),¹⁵ MnO₂/conductive polymer (0.2–7.7 Wh/kg),⁴⁵ and graphene/MnO₂/CNTs (3.2–8.9 Wh/kg).⁴⁶ In addition, the energy density could also be significantly improved by using the asymmetrical supercapacitor design. Further research is still under way. Moreover, the 3D graphene/MnO₂ composite network-based symmetrical supercapacitor exhibits an acceptable cycling stability performance over the range 0 to 1 V at a current density of 1.5 mA/cm² (Figure 4f). The capacitance decreased slightly from 29.8 F/g to 27.8 F/g after 500 cycles, and the Coulombic efficiency remained above 93%. After 5000 cycles, it retains a high specific capacitance of 24.2 F/g, about 82% of the Coulombic efficiency. The decrease of the capacitance is probably due to the mechanical expansion of MnO₂ during the ion insertion/removal process or the dissolution of some MnO₂ during the charge/discharge cycling. The cycling performance of the flexible supercapacitors for bending cycles, with a bending angle of 90°, was also tested, as shown in Figure 4f (inset); the resulting specific capacitance retained 92% of its initial value even after 200 bending actions, indicating its excellent mechanical and flexible properties.

CONCLUSIONS

We have developed a type of freestanding flexible 3D graphene/MnO₂ composite network as an

electrode for flexible supercapacitors. The freestanding, lightweight 3D graphene networks prepared from pressed Ni foam show superior mechanical strength and flexibility. A large and uniform mass of MnO₂ could be coated onto the entire skeleton by electrodeposition. This type of hybrid flexible electrode material shows remarkable electrochemical performance, with high specific capacitance, good rate capability, and extended cycling performance. These can be ascribed to the following features: (1) The high conductivity and porous structure of the 3D graphene networks serve as a double highway for electron transfer and easy access for electrolyte ions (Na⁺ in our case) to the electrode surfaces. This makes it an ideal supporter for active materials. (2) The good contact between the graphene and the MnO₂ nanomaterials produced by the electrochemical deposition process ensures low contact resistance and tight adhesion between them. Consequently, it can survive large and repeated bending deformations. (3) The high specific surface area of the 3D graphene networks means that even the thinnest MnO₂ layer in combination with its nanoporous structure gives a large active surface area and full accessibility for the electrolyte to the MnO₂ (Supporting Information, Table S1). This provides efficient use of the pseudocapacitive nanomaterial (MnO₂) for charge storage. On the basis of these intriguing features, the high-performance electrochemical behavior of the 3D graphene/MnO₂ composite network makes it a promising candidate as electrode material for a flexible supercapacitor. Furthermore, the simple and low-cost assembly of this flexible and lightweight supercapacitor means it presents potential applications, such as energy supply systems for small flying devices, adhesive tape-like supercapacitors, wearable supercapacitors, and so on.

EXPERIMENTS AND METHODS

Growth of the 3D Graphene Networks. Ni foam was used to catalyze the graphene growth. First, Ni foam (100 pores per inch, 380 g/m² surface density, and ~1.5 mm thick, purchased from Changsha Lyrun New Material Co. Ltd., China), cut into pieces of 1 cm × 2 cm, was pressed into a thin sheet ~0.2 mm thick. After being cleaned in 1 M HCl solution for 10 min and in acetone and deionized water for 15 min, respectively, the pressed nickel foam was prepared to grow graphene. Second, a typical growth process was as follows: (1) The standard 1.5 in. quartz tube was heated in a furnace up to 1000 °C under Ar gas flow; (2) nickel foam was introduced into the hot-zone of the furnace by moving the quartz tube under the H₂ (50 sccm) and Ar (280 sccm) gas flows and annealed for 20 min to clean their surfaces and eliminate a thin surface oxide layer; then a small amount of CH₄ (2.5 sccm) was introduced into the reaction tube under atmospheric pressure for 5 min growth; (3) the nickel foam was quickly cooled to 400 °C at a cooling rate of >300 °C/min under a H₂/Ar atmosphere by quickly removing it from the hot-zone of the furnace. Third, the Ni foams covered with graphene were drop-coated with a poly(methyl methacrylate)

(PMMA) solution (4.5% in anisole) and then baked at 160 °C for 0.5 h. The PMMA/graphene/Ni foam structure was obtained after solidification. Fourth, these samples were put into a 6 M HCl solution for 6 h to completely dissolve the Ni foam to obtain the PMMA/graphene, which was confirmed by X-ray photoelectron spectroscopy (XPS) spectra (Figure S10). Finally, three-dimensional graphene networks were obtained after removing PMMA in hot acetone at 40 °C.

Preparation of Graphene/MnO₂ Composite. Avoiding damaging the structure of 3D graphene networks, copper wires were embedded and connected to 3D graphene networks with silver paste, which enables a strong electrical contact and a small contact resistance between the copper wires and the 3D graphene networks. A piece of 1 cm × 1 cm 3D graphene network was immersed into a 20 mM Mn(NO₃)₂ and 100 mM NaNO₃ mixed aqueous solution. Electrochemical deposition of MnO₂ nanomaterials was performed with a three-electrode setup, where the conductive 3D graphene network was used as the working electrode, a platinum electrode as the counter electrode, and a Ag/AgCl electrode as the reference electrode. A square-wave pulse current of 500 μA/cm² with a period of 0.002 s and a duty ratio of 0.5 was applied to ensure the

conformal coating of nanostructured MnO_2 on the 3D graphene networks with a deposition time ranging from 15 to 1440 min. After electrodeposition, the composite was taken out and carefully washed with deionized water to remove excess electrolyte and then dried in a vacuum oven at 50 °C for 2 h. Finally, the composite was annealed under an Ar atmosphere at 300 °C to form crystalline MnO_2 . The mass of deposited MnO_2 nanomaterials was obtained by the weight difference of the networks before coating and after postannealing.

Electrochemical Measurement. In half-cell tests, a three-electrode configuration was used to measure the cyclic voltammetry, constant current charge/discharge behavior, and electrochemical impedance spectroscopy, where 3D graphene/ MnO_2 composite networks was used as the working electrode, Ag/AgCl as the reference electrode, and a piece of Pt as the counter electrode. In full cell tests, the flexible supercapacitor was assembled to measure the device performances. In detail, the 3D graphene/ MnO_2 composite network (area of 1 cm by 1 cm) with a mass loading of 0.4 mg/cm² was attached on the PET membrane (thickness of ~40 μm) as both electrodes and current collectors. Two pieces of these sheets were assembled with a ~120 μm thick membrane (DR2012, Suzhou Beige New Materials & Technology Co. Ltd.), as the separator, sandwiched in between (Figure 4a). The total thickness and weight of the devices were ~0.8 mm and less than 10 mg, respectively. The electrolyte used in all of the measurements was a 0.5 M Na_2SO_4 aqueous solution at pH 10.

Material Characterization. The morphologies of the obtained structures were characterized by field emission scanning electron microscopy (FE-SEM, Hitachi S-4800), with an accelerating voltage of 5 kV. The fine structures were characterized using transmission electron microscopy (FEI Tecnai F30, operated at 300 kV), X-ray diffraction (XRD, Philips, X'pert pro, Cu Ka, 0.154056 nm), and Raman spectroscopy (JY-HR800 micro-Raman, using a 532 nm wavelength YAG laser with a laser spot diameter of about 600 nm). The specific surface area was measured by the Brunauer–Emmett–Teller (ASAP 2020) method. The chemical component was analyzed on a PHI-5702 multi-functional X-ray photoelectron spectroscope, using Mg K α X-ray ($h\nu = 1253.6$ eV) as the excitation source. Electrical conductivities of our 3D graphene networks were measured by using the standard four-point probe technique (Loresta-GP, Mitsubishi Chemical). The mass of deposited MnO_2 nanomaterials was measured by a microbalance (Mettler, XS105DU). Electrochemical performance measurements were carried out at room temperature using an electrochemical workstation (RST5200, Zhengzhou Shiruisi Instrument Technology Co., Ltd., China).

Conflict of Interest: The authors declare no competing financial interest.

Acknowledgment. This work was financially supported by the National Natural Science Foundation of China (No. 61176058), partially by the Key Technology Research and Development Program of Gansu Province, China (No.1011GKCA027), and Natural Science Foundation of Gansu Province (1107RJYA280).

Supporting Information Available: Digital photographs and low- and high-magnification SEM images of 3D graphene networks and graphene/ MnO_2 composite; high-magnification TEM images of graphene; XRD patterns for graphene/ MnO_2 composite; XPS and the contact angle for bare 3D graphene networks; curves for electrical resistance of 3D graphene networks as a function of the number of bending cycles; table of surface area and specific capacitance (calculated for the entire electrode) of 3D graphene networks and graphene/ MnO_2 composites. This material is available free of charge via the Internet at <http://pubs.acs.org>.

REFERENCES AND NOTES

1. Lu, X.; Xia, Y. Electronic Materials: Buckling Down for Flexible Electronics. *Nat. Nanotechnol.* **2006**, *1*, 163–164.
2. Rogers, J. A.; Huang, Y. G. A Curvy, Stretchy Future for Electronics. *Proc. Natl. Acad. Sci. U. S. A.* **2009**, *106*, 10875–10876.
3. Nishide, H.; Oyaizu, K. Toward Flexible Batteries. *Science* **2008**, *319*, 737–738.
4. See www.enfucell.com/Products.htm.
5. Conway, B. E. *Electrochemical Supercapacitors: Scientific, Fundamentals and Technological Applications*; Plenum: New York, 1999; pp 19–20.
6. Miller, J. R.; Simon, P. Electrochemical Capacitors for Energy Management. *Science* **2008**, *321*, 651–652.
7. Simon, P.; Gogotsi, Y. Materials for Electrochemical Capacitors. *Nat. Mater.* **2008**, *7*, 845–854.
8. Pandolfo, A. G.; Hollenkamp, A. F. Carbon Properties and their Role in Supercapacitors. *J. Power Sources* **2006**, *157*, 11–27.
9. Chen, J.; Minett, A. I.; Liu, Y.; Lynam, C.; Sherrell, P.; Wang, C.; Wallace, G. G. Direct Growth of Flexible Carbon Nanotube Electrodes. *Adv. Mater.* **2008**, *20*, 566–570.
10. Ci, L.; Manikoth, S. M.; Li, X.; Vajtai, R.; Ajayan, P. M. Ultrathick Freestanding Aligned Carbon Nanotube Films. *Adv. Mater.* **2007**, *19*, 3300–3303.
11. Kim, C.; Choi, Y.-O.; Lee, W.-J.; Yang, K.-S. Supercapacitor Performances of Activated Carbon Fiber Webs Prepared by Electrospinning of PMDA-ODA Poly(Amide Acid) Solutions. *Electrochim. Acta* **2004**, *50*, 883–887.
12. Horng, Y.-Y.; Lu, Y.-C.; Hsu, Y.-K.; Chen, C.-C.; Chen, L.-C.; Chen, K.-H. Flexible Supercapacitor Based on Polyaniline Nanowires/Carbon Cloth with Both High Gravimetric and Area-Normalized Capacitance. *J. Power Sources* **2010**, *195*, 4418–4422.
13. Bi, R. R.; Wu, X. L.; Cao, F. F.; Jiang, L. Y.; Guo, Y. G.; Wan, L. J. Highly Dispersed RuO_2 Nanoparticles on Carbon Nanotubes: Facile Synthesis and Enhanced Supercapacitance Performance. *J. Phys. Chem. C* **2010**, *114*, 2448–2451.
14. Shan, Y.; Gao, L. Formation and Characterization of Multi-Walled Carbon Nanotubes/ Co_3O_4 Nanocomposites for Supercapacitors. *Mater. Chem. Phys.* **2007**, *103*, 206–210.
15. Yuan, L.; Lu, X.-H.; Xiao, X.; Zhai, T.; Dai, J.; Zhang, F.; Hu, B.; Wang, X.; Gong, L.; Chen, J.; et al. Flexible Solid-State Supercapacitors Based on Carbon Nanoparticles/ MnO_2 Nanorods Hybrid Structure. *ACS Nano* **2011**, *6*, 656–661.
16. Zhu, Y.; Murali, S.; Cai, W.; Li, X.; Suk, J. W.; Potts, J. R.; Ruoff, R. S. Graphene and Graphene Oxide: Synthesis, Properties, and Applications. *Adv. Mater.* **2010**, *22*, 3906–3924.
17. Choi, H.-J.; Jung, S.-M.; Seo, J.-M.; Chang, D. W.; Dai, L.; Baek, J.-B. Graphene for Energy Conversion and Storage in Fuel Cells and Supercapacitors. *Nano Energy* **2012**, *1*, 534–551.
18. Li, D.; Muller, M. B.; Gilje, S.; Kaner, R. B.; Wallace, G. G. Processable Aqueous Dispersions of Graphene Nanosheets. *Nat. Nanotechnol.* **2008**, *3*, 101–105.
19. Dikin, D. A.; Stankovich, S.; Zimney, E. J.; Pineri, R. D.; Domke, G. H. B.; Evmeneko, G.; Nguyen, S. T.; Ruoff, R. S. Preparation and Characterization of Graphene Oxide Paper. *Nature* **2007**, *448*, 457–460.
20. Chen, H.; Müller, M. B.; Gilmore, K. J.; Wallace, G. G.; Li, D. Mechanically Strong, Electrically Conductive, and Biocompatible Graphene Paper. *Adv. Mater.* **2008**, *20*, 3557–3561.
21. Lu, X.; Dou, H.; Gao, B.; Yuan, C.; Yang, S.; Hao, L.; Shen, L.; Zhang, X. A Flexible Graphene/Multiwalled Carbon Nanotube Film as a High Performance Electrode Material for Supercapacitors. *Electrochim. Acta* **2011**, *56*, 5115–5121.
22. Su, Q.; Liang, Y.; Feng, X.; Mullen, K. Towards Free-Standing Graphene/Carbon Nanotube Composite Films via Acetylene-Assisted Thermolysis of Organocobalt Functionalized Graphene Sheets. *Chem. Commun.* **2010**, *46*, 8279–8281.
23. Tai, Z.; Yan, X.; Lang, J.; Xue, Q. Enhancement of Capacitance Performance of Flexible Carbon Nanofiber Paper by Adding Graphene Nanosheets. *J. Power Sources* **2012**, *199*, 373–378.
24. Li, Z.; Mi, Y.; Liu, X.; Liu, S.; Yang, S.; Wang, J. Flexible Graphene/ MnO_2 Composite Papers for Supercapacitor Electrodes. *J. Mater. Chem.* **2011**, *21*, 14706–14711.
25. Wang, D.-W.; Li, F.; Zhao, J.; Ren, W.; Chen, Z.-G.; Tan, J.; Wu, Z.-S.; Gentle, I.; Lu, G. Q.; Cheng, H.-M. Fabrication of Graphene/Polyaniline Composite Paper via *in Situ* Anodic Electropolymerization for High-Performance Flexible Electrode. *ACS Nano* **2009**, *3*, 1745–1752.

26. Wu, Q.; Xu, Y.; Yao, Z.; Liu, A.; Shi, G. Supercapacitors Based on Flexible Graphene/Polyaniline Nanofiber Composite Films. *ACS Nano* **2010**, *4*, 1963–1970.

27. Zheng, J.; Ma, X.; He, X.; Gao, M.; Li, G. Preparation, Characterizations, and its Potential Applications of Pani/Graphene Oxide Nanocomposite. *Procedia Eng.* **2012**, *27*, 1478–1487.

28. Xu, Y.; Sheng, K.; Li, C.; Shi, G. Self-Assembled Graphene Hydrogel via a One-Step Hydrothermal Process. *ACS Nano* **2010**, *4*, 4324–4330.

29. Lee, S. H.; Kim, H. W.; Hwang, J. O.; Lee, W. J.; Kwon, J.; Bielawski, C. W.; Ruoff, R. S.; Kim, S. O. Three-Dimensional Self-Assembly of Graphene Oxide Platelets into Mechanically Flexible Macroporous Carbon Films. *Angew. Chem., Int. Ed.* **2010**, *49*, 10084–10088.

30. Choi, B. G.; Yang, M.; Hong, W. H.; Choi, J. W.; Huh, Y. S. 3D Macroporous Graphene Frameworks for Supercapacitors with High Energy and Power Densities. *ACS Nano* **2012**, *6*, 4020–4028.

31. Chen, Z.; Ren, W.; Gao, L.; Liu, B.; Pei, S.; Cheng, H.-M. Three-Dimensional Flexible and Conductive Interconnected Graphene Networks Grown by Chemical Vapour Deposition. *Nat. Mater.* **2011**, *10*, 424–428.

32. Dong, X.-C.; Xu, H.; Wang, X.-W.; Huang, Y.-X.; Chan-Park, M. B.; Zhang, H.; Wang, L.-H.; Huang, W.; Chen, P. 3D Graphene–Cobalt Oxide Electrode for High-Performance Supercapacitor and Enzymeless Glucose Detection. *ACS Nano* **2012**, *6*, 3206–3213.

33. Yu, G.; Hu, L.; Vosgueritchian, M.; Wang, H.; Xie, X.; McDonough, J. R.; Cui, X.; Cui, Y.; Bao, Z. Solution-Processed Graphene/MnO₂ Nanostructured Textiles for High-Performance Electrochemical Capacitors. *Nano Lett.* **2011**, *11*, 2905–2911.

34. Toupin, M.; Brousse, T.; Bélanger, D. Charge Storage Mechanism of MnO₂ Electrode Used in Aqueous Electrochemical Capacitor. *Chem. Mater.* **2004**, *16*, 3184–3190.

35. Lee, H.; Kang, J.; Cho, M. S.; Choi, J.-B.; Lee, Y. MnO₂/Graphene Composite Electrodes for Supercapacitors: The Effect of Graphene Intercalation on Capacitance. *J. Mater. Chem.* **2011**, *21*, 18215–18219.

36. Wu, Z.-S.; Ren, W.; Wang, D.-W.; Li, F.; Liu, B.; Cheng, H.-M. High-Energy MnO₂ Nanowire/Graphene and Graphene Asymmetric Electrochemical Capacitors. *ACS Nano* **2010**, *4*, 5835–5842.

37. Hou, Y.; Cheng, Y.; Hobson, T.; Liu, J. Design and Synthesis of Hierarchical MnO₂ Nanospheres/Carbon Nanotubes/Conducting Polymer Ternary Composite for High Performance Electrochemical Electrodes. *Nano Lett.* **2010**, *10*, 2727–2733.

38. Hu, L.; Chen, W.; Xie, X.; Liu, N.; Yang, Y.; Wu, H.; Yao, Y.; Pasta, M.; Alshareef, H. N.; Cui, Y. Symmetrical MnO₂–Carbon Nanotube–Textile Nanostructures for Wearable Pseudocapacitors with High Mass Loading. *ACS Nano* **2011**, *5*, 8904–8913.

39. Cao, X.; Shi, Y.; Shi, W.; Lu, G.; Huang, X.; Yan, Q.; Zhang, Q.; Zhang, H. Preparation of Novel 3D Graphene Networks for Supercapacitor Applications. *Small* **2011**, *7*, 3163–3168.

40. Yan, J.; Fan, Z.; Wei, T.; Qian, W.; Zhang, M.; Wei, F. Fast and Reversible Surface Redox Reaction of Graphene–MnO₂ Composites as Supercapacitor Electrodes. *Carbon* **2010**, *48*, 3825–3833.

41. Mao, L.; Zhang, K.; On Chan, H. S.; Wu, J. Nanostructured MnO₂/Graphene Composites for Supercapacitor Electrodes: the Effect of Morphology, Crystallinity and Composition. *J. Mater. Chem.* **2012**, *22*, 1845–1851.

42. Khomenko, V.; Raymundo-Piñero, E.; Béguin, F. Optimisation of an Asymmetric Manganese Oxide/Activated Carbon Capacitor Working at 2V in Aqueous Medium. *J. Power Sources* **2006**, *153*, 183–190.

43. Khomenko, V.; Raymundo-Piñero, E.; Frackowiak, E.; Béguin, F. High-Voltage Asymmetric Supercapacitors Operating in Aqueous Electrolyte. *Appl. Phys. A: Mater.* **2006**, *82*, 567–573.

44. Cottineau, T.; Toupin, M.; Delahaye, T.; Brousse, T.; Bélanger, D. Nanostructured Transition Metal Oxides for Aqueous Hybrid Electrochemical Supercapacitors. *Appl. Phys. A: Mater.* **2006**, *82*, 599–606.

45. Duay, J.; Gillette, E.; Liu, R.; Lee, S. B. Highly Flexible Pseudocapacitor Based on Freestanding Heterogeneous MnO₂/Conductive Polymer Nanowire Arrays. *Phys. Chem. Chem. Phys.* **2012**, *14*, 3329–3337.

46. Cheng, Y.; Lu, S.; Zhang, H.; Varanasi, C. V.; Liu, J. Synergistic Effects from Graphene and Carbon Nanotubes Enable Flexible and Robust Electrodes for High-Performance Supercapacitors. *Nano Lett.* **2012**, *12*, 4206–4211.